Chinese Chemical Letters 33 (2022) 4948–4951

Contents lists available at ScienceDirect

Chinese Chemical Letters

journal homepage: www.elsevier.com/locate/cclet

Insight into the *in vivo* fate of intravenous herpetrione amorphous nanosuspensions by aggregation-caused quenching probes

Lingyu Hang[a,b,1], Chengying Shen[c,1], Baode Shen[b,*], Hailong Yuan[a,b,*]

[a] Department of Pharmacy, Air Force Medical Center, PLA, Beijing 100142, China
[b] College of Pharmacy, Jiangxi University of Chinese Medicine, Nanchang 330004, China
[c] Department of Pharmacy, Jiangxi Provincial People's Hospital, Nanchang 330006, China

ARTICLE INFO

Article history:
Received 15 December 2021
Revised 27 March 2022
Accepted 29 March 2022
Available online 4 April 2022

Keywords:
Amorphous nanosuspensions
Herpetrione
In vivo fate
Intravenous delivery
Aggregation-caused quenching

ABSTRACT

Intravenous nanosuspensions are attracted growing attention as a viable strategy for development of intravenous formulations of poorly water-soluble drugs. However, only few information about the biological fate of intravenous nanosuspensions is currently known, especially amorphous nanosuspensions are not reported yet. In this study, the *in vivo* fate of herpetrione (HPE) amorphous nanosuspensions following intravenous administration was explored by using an aggregation-caused quenching (ACQ) probe and HPLC methods. The ACQ probe is physically embedded into HPE nanoparticles *via* anti-solvent method to form HPE hybrid nanosuspensions (HPE-HNSs) for bioimaging. HPE-HNSs emit strong and stable fluorescence, but fluorescence quenches immediately upon the dissolution of HPE-HNSs, confirming the self-discrimination of HPE-HNSs. Following intravenous administration of HPE-HNSs, integral HPE-HNSs and HPE show similar degradation and biodistribution, with rapid clearance from blood circulation and obvious accumulation in liver and lung. Due to the slower dissolution and enhanced recognition by reticuloendothelial system, 450 nm HPE-HNSs accumulate more in liver, lung and spleen than that of 200 nm HPE-HNSs. These results demonstrate that integral HPE-HNSs determine the *in vivo* performance of HPE-HNSs. This study provides insight into the *in vivo* fate of intravenous amorphous nanosuspensions.

Recently, intravenous nanosuspensions are attracted growing attention as a viable strategy for development of intravenous formulations of poorly water-soluble drugs [1,2]. Many studies have been performed to investigate the systemic delivery of nanosuspensions [3,4], and demonstrate the superiority of intravenous nanosuspensions over other intravenous nano-formulations, such as high drug loading, less toxicity, simple production process and universal adaptivity [5,6]. However, unlike the commercial success of a dozen oral preparations [7], only several parenteral nanosuspension are available on the market [8], which may be mainly associated with various challenges of parenteral nanosuspensions development, such as stability issues, potential toxicity of nanosuspensions accumulated in specific organs [6–11]. Currently, little information about the *in vivo* fate of intravenous drug nanosuspensions is known, leading to limited knowledge about their toxicity. Therefore, it is of tremendous importance to elucidate the *in vivo* fate of intravenous nanosuspensions, which may facilitate development and more commercial success of intravenous nanosuspensions.

Fortunately, a few researches have been performed to explore the *in vivo* fate of intravenous nanosuspensions and made some interesting findings [12,13]. By establishing physiologically based pharmacokinetic model, Dong *et al.* [12] demonstrated that intravenous nanosuspensions of SNX-2112 rapidly released drug molecules *in vivo*, exhibiting similar pharmacokinetic behaviors to drug co-solvent. However, different *in vivo* fates between paclitaxel nanosuspensions and solution (Taxol®) were found by tracking fluorescently hybrid nanosuspensions (HNSs), which was developed by embedding traces of near-infrared (NIR) fluorophores into the drug nanoparticles [13]. The paclitaxel HNSs were cleared rapidly from the blood circulation by the MPS and retained in the major organs (liver, lung, spleen and kidneys) for more than 48 h, while Taxol® was maintained in plasma longer, but distributed less to the major organs and significantly eliminated within 24 h Notably, along with the dissolution of paclitaxel HNSs *in vivo*, the NIR dyes were released but still emitted fluorescence, which may result in misunderstanding of the *in vivo* fate of paclitaxel HNSs.

In order to discriminate HNSs from released dyes, an aggregation-caused quenching (ACQ) probe was utilized to prepare

* Corresponding authors.
E-mail addresses: shenbaode@163.com (B. Shen), yhlpharm@126.com (H. Yuan).
[1] These authors contributed equally to this work.

https://doi.org/10.1016/j.cclet.2022.03.108
1001-8417/

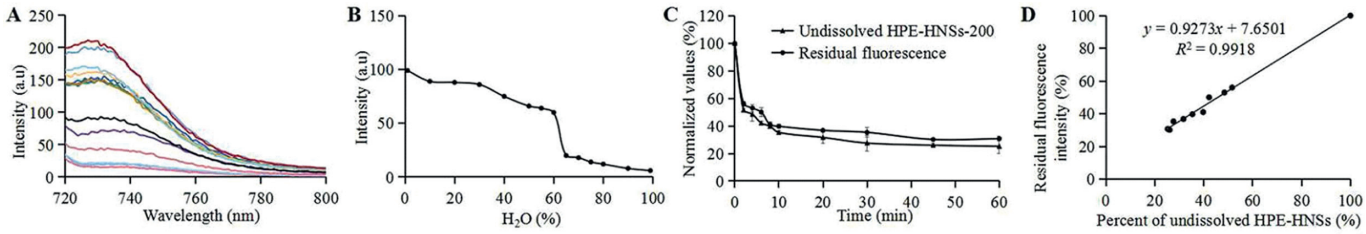

Fig. 1. Fluorescence emission spectra and fluorescence intensity of HPE-HNSs-200 in different water-ethanol solution systems (A). The change of the peak fluorescence intensity with the increase of water ratio (B). Normalized value of non-dissolved HPE-HNSs-200 and residual fluorescence intensity percentage *versus* time during dissolution (C). Correlation between dissolution and fluorescence quenching (D).

HNSs with self-discrimination for exploring their biological fate [14–20]. The ACQ probes hold a basic BODIPY or aza-BODIPY structure and are hydrophobic [21]. The probes can emit near infrared (NIR) fluorescence when molecularly embedded in HNSs, but absolute fluorescence quenching occurs when they are released to aqueous environments following the dissolution of HNSs, resulting from their self-aggregation due to intermolecular π-π stacking in aqueous solution [14,18]. Therefore, the observed fluorescence signal can be representative Aof integral HNSs due to the complete elimination of free-probe interference. The ACQ probe has also been employed for exploring the *in vivo* fate of a series of drug nanocarriers [21–27]. By using ACQ probes, intravenous curcumin nanosuspensions were demonstrated to be rapidly cleared from blood and accumulated mainly in liver and lung for at least 48 h [16]. Our group found that quercetin nanosuspensions exhibited similar *in vivo* behavior to that of curcumin nanosuspensions following intravenous administration [15]. However, the *in vivo* fate of different drugs nanosuspensions may be drastically distinct due to their various physicochemical properties [28]. Only few studies are focus on the crystalline nansuspensions, the *in vivo* fate of intravenous amorphous nanosuspensions is not reported yet.

Therefore, the present study was designed to explore the *in vivo* fate of amorphous nanosuspensions following intravenous delivery. Herpetrione (HPE, Fig. S1A in Supporting information), a promising and potent anti-hepatitis virus agent with poor water solubility that extracted from the seeds of *Herpetospermum caudigerum* Wall., was used as model drug [29,30]. The HPE-HNSs were prepared by anti-solvent method using ACQ probe for live and *ex vivo* imaging, while the HPE concentrations in plasma and main organs were also determined.

HPE-HNSs with particle size around 200 nm (HPE-HNSs-200) and 450 nm (HPE-HNSs-450) were successfully prepared. Their physicochemical properties are shown in Table S1 and Fig. S1 (Supporting information). HPE-HNSs-200 and HPE-HNSs-450 got average diameter of 201 nm and 454 nm, respectively, with PDI less than 0.2 (Fig. S1B), indicating narrow size distribution [18]. Besides, HPE-HNSs-200 and HPE-HNSs-450 show similar fluorescent intensities that more than 1.0×10^{10} [p/s]/[μW/cm²]. Both of HPE-HNSs-200 and HPE-HNSs-450 are spherical under SEM (Figs. S1C and D). No significant diffraction peaks are seen from the powder X-ray diffraction patterns of HPE-HNSs and HPE raw material (Fig. S1E), indicating their amorphous state.

In order to accurately monitor the *in vivo* fate of HPE-HNSs, HPE-HNSs must have desired properties including good fluorescence stability, high water-quenching sensitivity and good synchronicity between the dissolution of HPE-HNSs and fluorescence quenching [14,18]. The fluorescence stability of HPE-HNSs-200 in deionized water, phosphate buffers (pH 7.4) and rat plasma is shown in Fig. S2A (Supporting information). The fluorescence intensities of HPE-HNSs-200 remain relatively constant in deionized water and phosphate buffers, with the fluorescence kept more than 80% over 48 h, indicating quite stable of HPE-HNSs-200. About 20% decrease of fluorescence intensity can be attributed to the dissolution of HPE-HNSs-200. More declination of fluorescence intensity in plasma (about 30%) may be due to possible interactions of the components in the plasma with HPE-HNSs, facilitating the dissolution of HPE-HNSs [31]. A high water sensitivity of the fluorescence is observed upon the dissolution of HPE-HNSs-200. As shown in Figs. 1A and B, the fluorescence of HPE-HNSs-200 declines slowly as water increases to 60%, but sharply diminishes when the water content increases from 60% to 80%, and quenches completely when the water is around 80%. Figs. 1C and D show a good linear correlation between undissolved HPE-HNSs-200 and residual fluorescence intensities with correlation coefficients exceeding 0.9, indicating good synchronicity between the dissolution of HPE-HNSs-200 and fluorescence quenching. Similar results are observed for HPE-HNSs-450 (Figs. S2B-F in Supporting information). These results suggest that fluorescent signals of ACQ probes can represent integral HNSs and be used for tracking intact HPE-HNSs.

Animal care and experimental procedures were followed the NIH Guidelines for the Care and Use of Laboratory Animals and approved by the Institution Ethical Committee of Air Force Medical Center, PLA of China (No. 2020–148-PJ01). Following intravenous administration, obvious fluorescent signals are observed in blood for both of HPE-HNSs-200 and HPE-HNSs-450 (Fig. S3 in Supporting information), with fluorescence retained in blood more than 12 h. Figs. 2A and C show that the fluorescence decreases rapidly from 5 min to 4 h and slowly thereafter to 36 h. Only 15.64% and

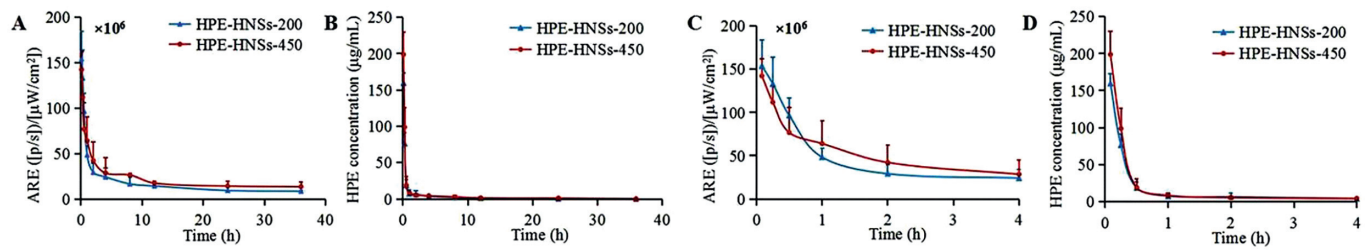

Fig. 2. Kinetic profiles of HPE-HNSs (A) and pharmacokinetic curves of HPE (B) following intravenous administration of HPE-HNSs. Enlargement of the kinetic profiles of HPE-HNSs (C) and pharmacokinetic curves of HPE (D) within 0–4 h The HPE-HNSs in kinetic profiles were expressed by quantifying average radiant efficiency (ARE) of different time point blood samples.

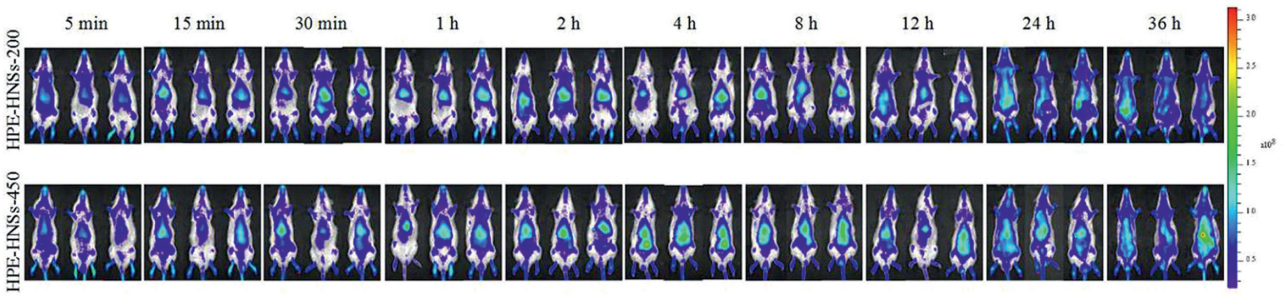

Fig. 3. Live imaging of fluorescence for rats after intravenous administration of HPE-HNSs.

20.05% fluorescence remains in blood circulation at 4 h for HPE-HNSs-200 and HPE-HNSs-450 as compared to the fluorescence measured at 5 min, demonstrating rapid clearance of integral HPE-HNSs from blood circulation. HPE concentrations fall faster as compared to fluorescence, only about 4% of HPE remains in plasma at 1 h for both of HPE-HNSs-200 and HPE-HNSs-450 (Figs. 2B and D). The main pharmacokinetics parameters of fluorescence intensity and HPE are shown in Tables S2 and S3 (Supporting information). The $AUC_{0\text{-}t}$ and $MRT_{0\text{-}t}$ of HPE-HNSs-450 based on average radiant efficiency (ARE) are higher than that of HPE-HNSs-200, which may be due to the slower dissolution of the larger nanosuspensions [32]. The pharmacokinetics parameters of HPE show no significant difference between HPE-HNSs-200 and HPE-HNSs-450.

Live imaging shows the translocation of integral HPE-HNSs *in vivo* following intravenous administration (Fig. 3). Both of HPE-HNSs-200 and HPE-HNSs-450 are pervasively distributed throughout the body until 36 h, with high accumulation in the abdominal area, mapping reticulo-endothelial system (RES) organs. HPE-HNSs-450 seems to accumulate more in the abdominal area (RES organs) of rats as compared HPE-HNSs-200. These results demonstrate that intravenous HPE-HNSs are mainly captured by RES organs and the larger ones are captured in more amounts. The slower dissolution of HPE-HNSs-450 may also contribute its more retention of fluorescence *in vivo*. Similar results were reported in previous studies with intravenous administration of curcumin HNSs and quercetin HNSs [15,16]. Fluorescence intensity appeared to be increasing after 24 h, which might be caused by the reillumination of fluorescence, but this does not significantly interfere with the judgment of the results [18].

Fig. 4A shows the *ex vivo* fluorescent images of major organs following intravenous administration of HPE-HNSs. The fluorescent signals appear in all detected organs (heart, liver, spleen, lung and kidney) along with the blood flow, with obvious accumulation in liver, lung and spleen and less distribution in other organs, indicating high accumulation of integral HPE-HNSs in RES organs. This can be ascribed to the recognition and phagocytosis of macrophages residing in RES organs [33]. The drastically high accumulation of HPE-HNSs in RES organs is in coincidence with the rapid clearance of HPE-HNSs from circulation as indicated by pharmacokinetics study. Both of HPE-HNSs-200 and HPE-HNSs-450 stay in liver and lung for at least 36 h HPE-HNSs-450 shows stronger fluorescence in liver as compared to HPE-HNSs-200, and the fluorescence in liver peaks at around 2 h for HPE-HNSs-200, while about 4 h for HPE-HNSs-450. The faster phagocytic uptake of smaller nanoparticles by liver tissue may contribute to the rapid peaking of HPE-HNSs-200 [34], and the faster dissolution of HPE-HNSs-200 due to its smaller size leads to less fluorescence retention in liver [35].

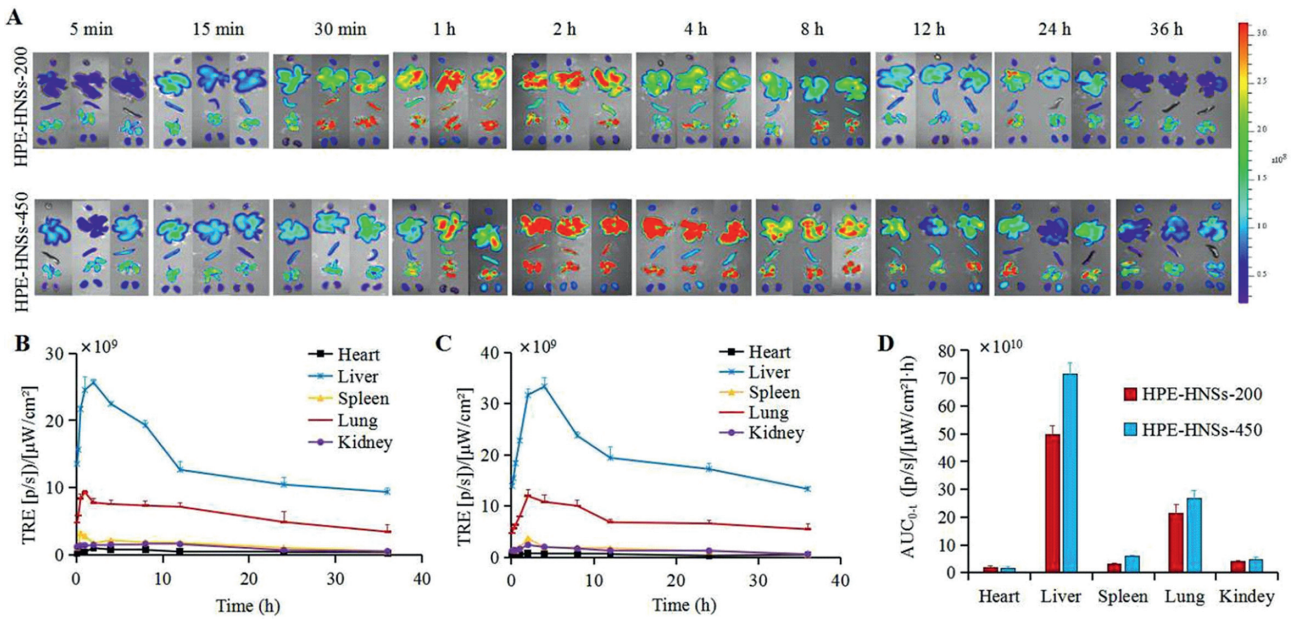

Fig. 4. *Ex vivo* imaging of organs after intravenous administration of HPE-HNSs (A). The heart, liver, spleen, lungs, and kidneys are shown from top to bottom in each picture. Fluorescence quantification of total radiant efficiency (TRE) of main organs after intravenous injection of HPE-HNSs-200 (B) and HPE-HNSs-450 (C). $AUC_{0\text{-}t}$ of the integral HPE-HNSs distribution in organs following intravenous administration (D).

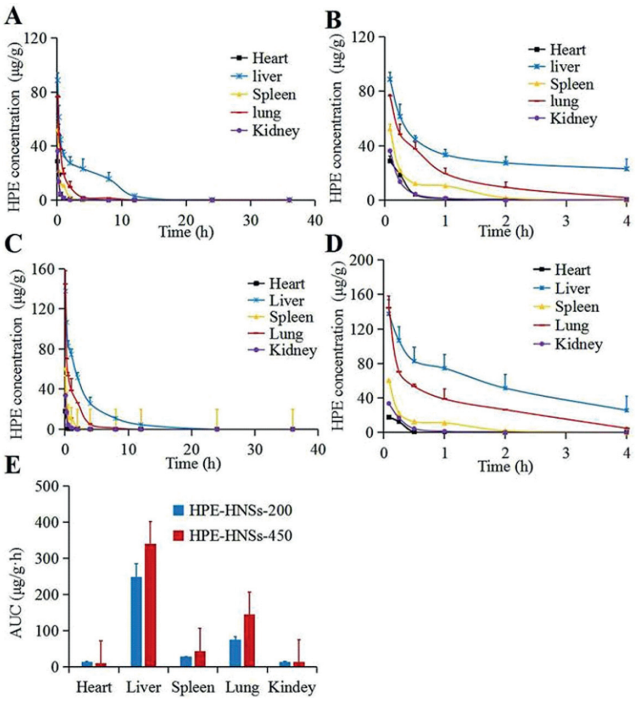

Fig. 5. Mean HPE concentration-time curves in organs for rats after intravenous administration of HPE-HNSs-200 (A and B) and HPE-HNSs-450 (C and D). Enlargement of the Mean HPE concentration-time curves in organs for rats within 0–4 h (B and D). AUC_{0-t} of the HPE distribution in organs following intravenous administration (E).

The fluorescent intensity of each organ was quantified by regions of interest (ROI) method based on total radiant efficiency (TRE) (Figs. 4B and C). The TRE values in liver present a trend of rapid increment and gradual drop for both of HPE-HNSs-200 and HPE-HNSs-450, but display different peak times. The TRE values in lung show similar increase trend to liver, but decline more slowly. The AUC_{0-t} based on TRE was calculated by Pharmacokinetic software DAS2.0 using statistical moment model (Fig. 4D). The AUC_{0-t} in various organs shows an order of liver > lung > spleen ≈ kidney > heart. As the volume of liver is the biggest among the tested organs, the liver is undoubtedly the major destination of HPE-HNSs. By calculation of AUC_{0-t}, about 85% of integral HPE-HNSs accumulate in liver and lung for both of HPE-HNSs-200 and HPE-HNSs-450 among all tested organs, further confirming high accumulation of integral HPE-HNSs in RES organs.

HPE concentrations in each organ were determined by HPLC (Figs. 5A-D). No increase tendency but faster decline is observed in the profiles of HPE in various organs for both of HPE-HNSs-200 and HPE-HNSs-450, which is inconsistent with the TRE values. The AUC_{0-t} of HPE concentrations is in the following order: liver > lung > spleen > kidney ≈ heart (Fig. 5E). The distributions of HPE in liver and lung are similar to the TRE, but are different in spleen, kidney and heart. This may be due to that the detected HPE in various organs include integral HPE-HNSs and released HPE molecules, while the observed fluorescence only reflects the undissolved or partially dissolved HPE-HNSs but not released HPE. HPE-HNSs dissolve continuously *in vivo*, but differently in various time, therefore, the released HPE may account for major contribution for the distribution of HPE-HNSs in some time points or organs. HPE-HNSs-450 shows significantly higher AUC_{0-t} in liver, lung and spleen than those of HPE-HNSs-200 for both of TRE and HPE concentrations. The enhanced accumulation of HPE-HNSs-450 may be attributed to the slower dissolution rate and enhanced recognition by RES [33].

In conclusion, the ACQ probe is proven to represent integral HPE-HNSs and can be used for accurately monitoring the *in vivo* fate of HPE-HNSs. Following intravenous administration of HPE-HNSs, integral HPE-HNSs are rapidly cleared from the blood circulation, with obvious accumulation in liver, lung and spleen and less distribution in other organs. HPE concentrations are found similar degradation in blood and biodistribution characteristics to integral HPE-HNSs. Due to the slower dissolution and enhanced recognition by RES, HPE-HNSs-450 accumulate more in liver, lung and spleen as compared to HPE-HNSs-200. These results demonstrate that integral HPE-HNSs determine the *in vivo* performance of HPE-HNSs. Our study provides insight into the *in vivo* fate of intravenous amorphous nanosuspensions.

Declaration of competing interest

The authors declare that they have no known competing financial interests or personal relationships that could have appeared to influence the work reported in this paper

Acknowledgment

This work was supported by the National Natural Science Foundation of China (Nos. 81873092, 81573697, 82174074, 81803741).

Supplementary materials

Supplementary material associated with this article can be found, in the online version, at doi:10.1016/j.cclet.2022.03.108.

References

[1] S. Jacob, A.B. Nair, J. Shah, Biomater. Res. 24 (2020) 3.
[2] D. Patel, S.S. Zode, A.K. Bansal, Int. J. Pharm. 586 (2020) 119555.
[3] Z.L. Wang, Z.W. Li, D. Zhang, L. Miao, G.H. Huang, Drug Deliv. 22 (2015) 79–85.
[4] Y. Lu, J.P. Qi, X. Dong, W. Zhao, W. Wu, Drug Discov. Today 22 (2017) 744–750.
[5] N.P. Aditya, H.J. Yang, S. Kim, S. Ko, Colloids Surf. B: Biointerfaces 127 (2015) 114–121.
[6] R.D. Bachu, P. Chowdhury, Z.H. Al-Saedi, P.K. Karla, S.H. Boddu, Pharmaceutics 10 (2018) 28.
[7] V.K. Pawar, Y. Singh, J.G. Meher, S. Gupta, M.K. Chourasia, J. Control. Release 183 (2014) 51–66.
[8] Y. Lu, Y. Chen, R.A. Gemeinhart, W. Wu, T.L. Li, Nanomedicine 10 (2015) 2537–2552.
[9] L.L. Wang, J. Du, Y.Q. Zhou, Y.C. Wang, Nanomedicine 13 (2017) 455–469.
[10] A. Madni, M.A. Rahem, N. Tahir, Int. J. Pharm. 530 (2017) 326–345.
[11] A. Tuomela, J. Hirvonen, L. Peltonen, Pharmaceutics 8 (2016) 16.
[12] D. Dong, X. Wang, H. Wang, et al., Int. J. Nanomedicine 10 (2015) 2521–2535.
[13] C.P. Hollis, H.L. Weiss, M. Leggas, et al., J. Control. Release 172 (2013) 12–21.
[14] C.Y. Shen, Y.Q. Yang, B.D. Shen, et al., Nanoscale 10 (2017) 436–450.
[15] B.D. Shen, C.Y. Shen, W.F. Zhu, H.L. Yuan, Acta Pharm. Sin. B 11 (2021) 978–988.
[16] T. Wang, J.P. Qi, N. Ding, et al., Int. J. Pharm. 546 (2018) 10–19.
[17] T.T. Shi, Y.J. Lv, W.Z. Huang, et al., Int. J. Pharm. 588 (2020) 119737.
[18] Y.K. Xie, B.K. Shi, F. Xia, et al., J. Control. Release 270 (2018) 65–75.
[19] D.L. Liu, B. Wan, J.P. Qi, et al., Chin. Chem. Lett. 29 (2018) 1834–1838.
[20] Y.Q. Yang, Y.J. Lv, C.Y. Shen, et al., Acta Pharm. Sin. B 11 (2021) 1056–1068.
[21] H.S. He, L.T. Wang, Y.H. Ma, et al., J. Control. Release 327 (2020) 725–736.
[22] L. Zoya, H.S. He, L.T. Wang, et al., Chin. Chem. Lett. 32 (2021) 1545–1549.
[23] J.P. Qi, X.W. Hu, X.C. Dong, et al., Adv. Drug. Deliv. Rev. 143 (2019) 206–225.
[24] H.S. He, S.F. Jiang, Y.C. Xie, et al., Nanoscale Horiz. 3 (2018) 397–407.
[25] F. Xia, W.F. Fan, S.F. Jiang, et al., ACS Appl. Mater. Interfaces 9 (2017) 21660–21672.
[26] E. Ahmad, Y.H. Feng, J.P. Qi, et al., Nanoscale 9 (2017) 1174–1183.
[27] X.W. Hu, J. Zhang, Z. Yu, et al., Nanomedicine11 (2015) 1939–1948.
[28] J.F. Zhang, C.D. Corpstein, T.L. Li, Acta Pharm. Sin. B 11 (2021) 1021–1029.
[29] J.J. Guo, P.F. Yue, J.L. Lv, et al., Int. J. Pharm. 441 (2013) 227–233.
[30] B.D. Shen, C.Y. Shen, X.D. Yuan, et al., Eur. J. Pharm. Biopharm. 85 (2013) 1348–1356.
[31] T. Chen, C. Li, Y. Li, et al., Mol. Pharm. 13 (2016) 3864–3875.
[32] X.H. Wang, Y. Liu, C.Y. Shen, et al., J. Drug Deliv. Sci. Tec. 52 (2019) 778–783.
[33] J.L. Yang, Z.R. Dong, W.J. Liu, et al., Chin. Chem. Lett. 29 (2020) 875–879.
[34] C.G. Park, Y.K. Kim, M.J. Kim, J. Control. Release 220 (2015) 180–188.
[35] G.P. Liu, D.R. Zhang, Y. Jiao, et al., Colloids Surf. B 102 (2013) 620–626.